Binding Energies of the Neutral and Ionic Clusters of Naphthalene in Their Ground Electronic States

Takashige Fujiwara and Edward C. Lim*,†

Department of Chemistry and The Center for Laser and Optical Spectroscopy, The University of Akron, Akron, Ohio 44325-3601

Received: December 16, 2002; In Final Form: March 24, 2003

The binding energies of the neutral and ionic clusters of naphthalene have been determined from the two-color two-photon measurements of the ionization potentials and appearance potentials. The measured binding energies (D_0) of the neutral dimer is significantly smaller than the binding energies (D_e) computed by correlated (MP2) quantum chemistry calculations. Interestingly, the experimental binding energy of the naphthalene dimer ion is very close to half the transition energy of its charge resonance absorption band, indicating that the dimer ion is stabilized mostly by charge resonance interactions. The slow increase in the dimer ion current with increasing photon energy, near the threshold of the excimer-mediated photoionization, suggests that the geometry of the dimer ion is significantly different from the sandwich-pair geometry of the excimer. Finally, the measured evaporation energies of the neutral tetramer, trimer ion, and tetramer ion support the trimer core structure of the neutral tetramer and the dimer core structure of the ionic clusters.

Introduction

As the species formed by intermolecular interactions, the geometrical structures and binding energies of the van der Waals (vdW) dimers and higher clusters of aromatic hydrocarbons provide fundamental understanding of aromatic−aromatic interactions that play important roles in many chemical and biological systems. Although much has been written about the structures and binding energies of benzene dimers,[1] neither the structure nor the binding energy is known for naphthalene dimer, which is the prototype of the vdW dimers of polycyclic aromatic hydrocarbons. This is unfortunate since accurate experimental data can provide crucial tests of the reliability of the ab initio and other theoretical methods that have been used to describe the intermolecular potential of the neutral dimer[2−5] and dimer ion[5] of naphthalene.

In this paper, we report the experimental measurements of the binding energies of the small neutral and ionic clusters of naphthalene and their comparison to the theoretical predictions (for neutral clusters) and to the previous experimental data (for ionic clusters). The results provide significant new information concerning the intermolecular forces that bind the neutral and ionic clusters of aromatic hydrocarbons.

Experimental Section

Following the work of Neusser and co-workers on benzene clusters[6,7] and that of Grover et al. on benzene dimer,[8] the binding energies of the ground-state neutral clusters A_n were determined from the evaporation energy $E_{evp}(n)$, which is the energy of required to evaporate one neutral monomer from the n-mer cluster, i.e., $A_n \rightarrow A_{n-1} + A$. The $E_{evp}(n)$ is related to the appearance potential AP_n of the metastable dissociation channel leading to the formation of the fragment ion A_{n-1}^+, and the ionization potential $IP(n-1)$ of the ground-state neutral cluster A_{n-1}, by $E_{evp}(n) = AP(n) - IP(n-1)$, as shown in Figure 1. The sum of the evaporation energy $\sum_{i=2}^{n} E_{evp}(i)$ yields the binding energy (dissociation energy) $D_0(n)$ of the cluster. Similarly, the evaporation energy $E_{evp}^+(n)$ of the ionic cluster A_n^+ can be determined from the difference between the appearance potential and the ionization potential of the neutral cluster A_n, i.e., $E_{evp}^+(n) = AP(n) - IP(n)$, Figure 1. Again, the sum of the evaporation energies $\sum_{i=2}^{n} E_{evp}^+(i)$ yields the binding energy $D_0^+(n)$ of the ionic cluster. For the neutral dimer, the binding energy can therefore be determined from the measurement of the AP of the dimer and IP of the monomer, whereas the binding energy of the dimer cation can be deduced from the measurement of the AP and IP of the neutral dimer.

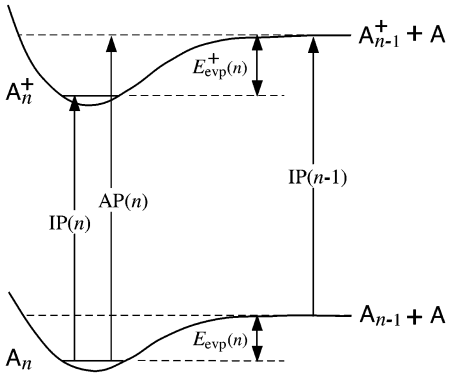

Figure 1. Schematic energy level diagram that relates the appearance potential (AP) and the ionization potential (IP) with the evaporation energy (the threshold energy needed for the evaporation of a neutral monomer, A) of the neutral (A_n) and ionic clusters (A_n^+).

The apparatus used to measure the APs and IPs is a differentially pumped angular-reflectron time-of-flight (ARTOF) mass spectrometer (Jordan D-850) of Wiley−McLaren design, which is coupled with a pulsed molecular beam source and two tunable ultraviolet (UV) dye lasers (Lambda Physik ScanMate 2E) pumped by separate Nd:YAG/excimer lasers (Continuum NY61-10/Quanta Ray GCR-150-10/Lambda Physik COM-

† Holder of the Goodyear Chair in Chemistry at The University of Akron. E-mail: elim@uakron.edu. Fax: (330) 972-6407.

10.1021/jp022605i CCC: $25.00
Published on Web 05/10/2003

Pex102). The timing of the photoionization laser with respect to the pump laser was accomplished electronically by synchronizing the firing of both lasers by the use of a delay generator (Stanford DG-535). Typically, photoionization (probe) laser was delayed by up to 200 ns with respect to excitation (pump) laser. The two UV laser beams were aligned collinearly, in some cases arranged in a counterpropagating pump−probe configuration, and mildly focused into a skimmed molecular-beam sample in the ion-acceleration region of the ARTOF mass spectrometer.

The pulsed molecular beam was formed by expanding a seeded naphthalene (heated to about 80 °C) in He at a backing pressure of up to 7 atm through a solenoid-driven valve (General Valve Series 9) with orifice of 0.2 mm. The molecular beam was skimmed by a conical skimmer (1 mm orifice) at a distance of about 4 cm downstream of the expansion source, and intersected the excitation field at a total distance of about 12 cm from the expansion orifice. The photoions formed by two-color resonant two-photon photoionization (2C-R2PI) were accelerated by a two-stage electric field configuration (ionization electric field of 135 V/cm) in a direction perpendicular to both the molecular beam and laser-field propagation directions and reflected at an ion reflectron, where a dual microchannel plate arrangement finally detected the reflected ions. The output of the detector was amplified and then fed to a 500 MHz transient digitizer (LeCroy LT342) controlled by a computer for storing and averaging photoions. By putting digital-gates at multiple mass-channels of photoion current it is possible to obtain mass-selected photoionization spectra while scanning laser wavelength.

To measure the ionization threshold, the pump laser at a fixed frequency (υ_1) excites a specific ground-state neutral cluster (e.g., dimer) into a vibronic level of the first electronic excited (S_1) state. A time-delayed pulses from the probe laser ionizes the electronically-excited neutral cluster. Scanning the ionization (probe) laser, with the pump laser set to a specific vibronic $S_1 \leftarrow S_0$ transition, gives a plot of photoion current as a function of two-photon energy $h(\upsilon_1 + \upsilon_2)$. The intercept of this plot (photoionization efficiency curve) with the baseline is subsequently taken as an onset of the IP. For measurement of the APs of those clusters, the reflectron in the ARTOF was operated in the partial collecting mode, in which the daughter ions produced by a metastable decay in the drift region appear comparably to the stable parent intensity. This mode was established by decreasing the reflectron potential ($U_d + U_{ref}$) slightly below the acceleration potential (U_{acc}). For the determination of the AP (i.e., the threshold energy needed for the evaporation of a neutral monomer from the cluster cation), the photoion signal of the daughter ion from the metastable decay channel was monitored as a function of the two-photon energy (above the ionization potential of the neutral cluster A_n).

To improve the signal-to-noise (S/N) ratio and to obtain more reliable measurements of IPs and APs, we performed the following routines in the data sampling. First, we set a time-delay between the pump and the probe laser so as to reduce an interference with photoion current generated by the pump laser alone via the one-color resonant two-photon photoionization (1C-R2PI). Second, we have implemented a new active-baseline subtraction (ABS) sampling method, which is similar to phase sensitive detection. This technique can actively extract contribution associated with the pump−probe sequence from that of the ion current generated by the probe laser alone via the 1C−R2PI process. To facilitate the ABS, we have operated the pump laser at half the repetition rate (e.g., 10 Hz) of both the probe laser and the pulsed nozzle (e.g., 20 Hz), so that the pump−probe sequence is established in alternate laser shots. The averaged signals from 1000 laser shots are stored at each scanning laser wavelength. Subtraction of one from the other yields an exact signal pertaining to the pump−probe sequence measurement. Despite the ABS sampling method used, it is not possible to rule out contribution (to signal) of ions produced by fragmentation of larger clusters by absorption of three or more photons. A careful adjustments of the two laser powers as well as the supersonic jet condition (to produce predominately a cluster-size of interest) were necessary to minimize such contributions. In the measurement of IPs the pump laser was typically kept at lower fluence (<50 μJ/pulse) than that of probe power (200 μJ/pulse), whereas for the measurement of APs the fluence of the pump laser was higher (100 μJ/pulse) than that of the probe (<30μJ/pulse) laser.

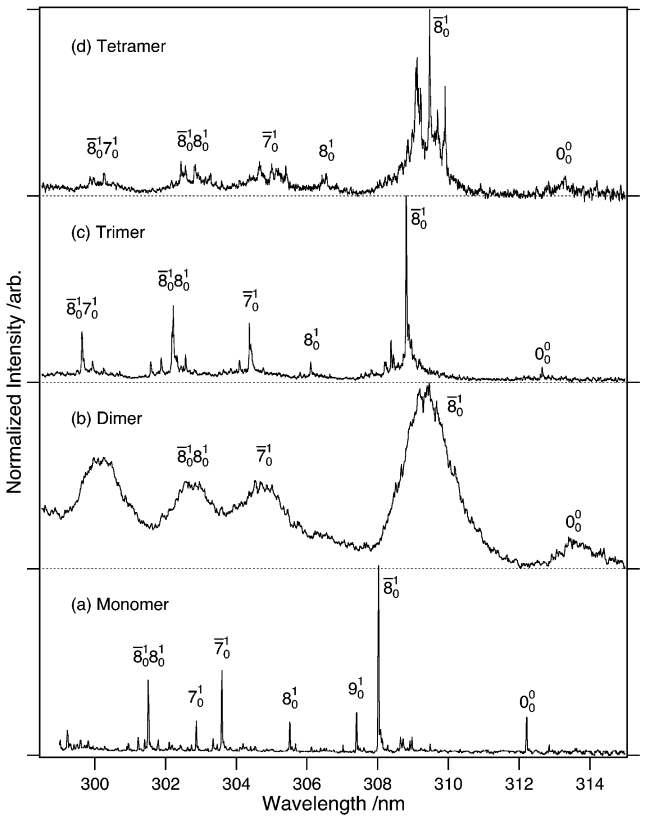

Figure 2. Two-color R2PI spectrum of (a) naphthalene monomer, and the one-color R2PI spectra of (b) dimer, (c) trimer, and (d) tetramer, showing their $S_1 \leftarrow S_0$ vibronic transitions. All spectra are normalized to the laser powers and displayed with the same peak intensities.

Results

The low-lying $S_1 \leftarrow S_0$ vibronic bands of the neutral naphthalene and its clusters obtained by the 2C/1C−R2PI are shown in Figure 2 in which the vibronic band assignments are based on notations of Stockburger et al.[9] Figure 3 presents the reflectron TOF mass spectrum of naphthalene cluster ions, obtained by one-color two-photon ionization at ($\lambda = 297.5$ nm). The features due to the stable parent ions and the daughter ions formed from the metastable decays are indicated in the spectrum. The metastable peaks and the parent ion peaks are well separated, so that the ionization potential and the appearance potential for monomer evaporation can be measured without interference from the other.

Figure 4 shows the ionization thresholds for the cluster and monomer ions, measured by two-color two-photon ionization.

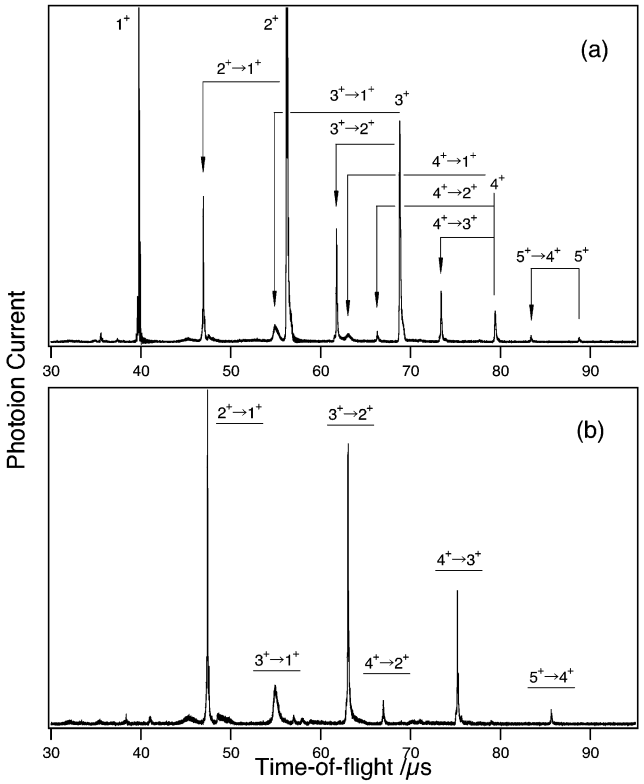

Figure 3. (a) Angular-reflectron time-of-flight (ARTOF) mass spectrum of naphthalene cluster ions obtained by operating the ARTOF instrument in the partial-collection mode. The vertical arrows indicate the daughter ion peaks produced by their metastable decay in the drift region. The observed decay channels are given by the horizontal arrows. (b) Pure metastable mass spectrum corresponding to the above partial-collected spectrum. The laser wavelength for the both spectra with the 2C−R2PI was set at $\lambda = 297.5$ nm.

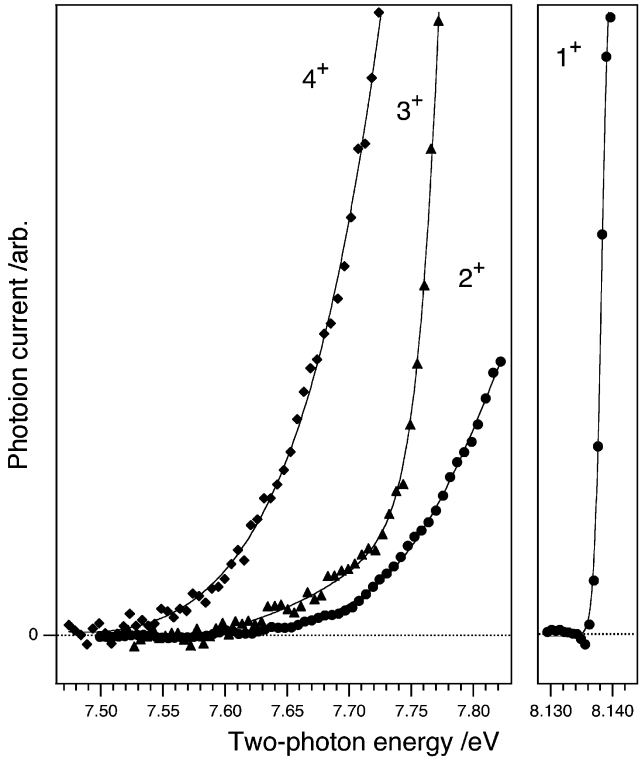

Figure 4. Photoionization efficiency curves on naphthalene and its clusters ($n = 1-4$) as a function of two-photon energy in the vicinity of the ionization threshold. The pump laser was tuned to the respective $\bar{8}_0^1$ bands of naphthalene and the clusters. The ionization potential is taken as an onset of the photoion current.

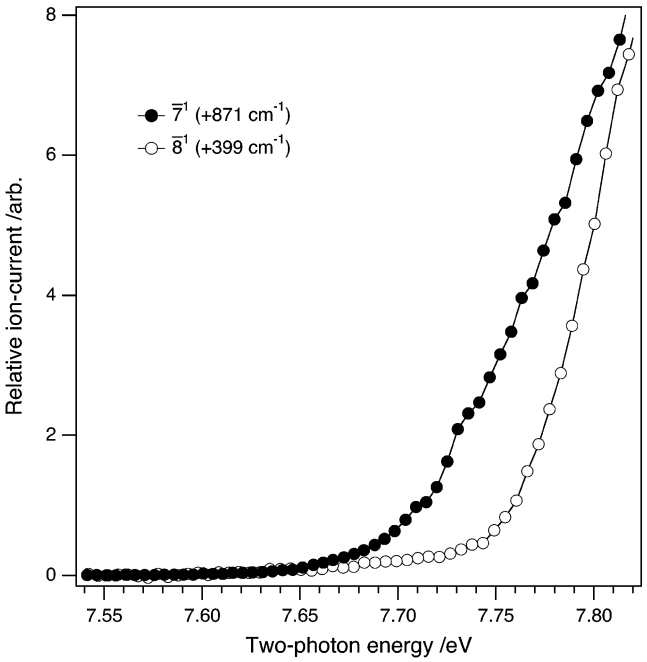

Figure 5. Dependence of the ionization efficiency on the initially-excited S_1 vibronic level of naphthalene trimer. Excitation of the higher-energy S_1 level $\bar{7}^1$ ($0^0 + 871$ cm^{-1}) is known to lead to a rapid excimer formation (refs 11 and 12).

As in the case of the benzene clusters studied by Neusser and coworkers,[10] the ion intensity increases slowly with increasing two-photon energy, near the threshold. For the dimer, the photon energy dependence of the photoionization efficiency does not depend on the time delay between the pump laser and probe (ionization) laser, or the nature of the initial S_1 vibronic level prepared by the pump laser. This is expected as the S_1 dimer of naphthalene exhibits barrierless excimer formation,[11,12] so that the intermediate of the two-photon ionization is the excimer, independent of the time delay between the pump and the ionization lasers. To probe the effect of excimer formation on the build-up rate of the photoion yield near threshold, the two-photon ionization experiments were carried out for the naphthalene trimer by pumping the $\bar{7}^1$ ($0^0 + 871$ cm^{-1}) and $\bar{8}^1$ ($0^0 + 399$ cm^{-1}) levels of the trimer $S_1 \leftarrow S_0$ absorption that respectively lie above and below the energy threshold for excimer formation.[11,12] The results, presented in Figure 5, show that the rate of increase in ion current with increasing photon energy, near threshold, is much smaller for excitation of the $\bar{8}^1$ level than for excitation of the higher energy $\bar{7}^1$ level that leads to excimer formation. The adiabatic ionization potentials of $(C_{10}H_8)_n$, $n = 1-4$, obtained from the intercept of the photocurrent signal with the baseline, are listed in Table 1.

The measurements of the appearance potentials are more problematic, as the metastable drift peak intensities of the monomer evaporation from the cluster ions are much weaker than the parent ion intensities, especially for the dimer. Wavelength-by-wavelength signal averaging of the fragment ion signal, normalized to the parent ion intensity, is therefore needed to determine the appearance potential. A typical measurement is illustrated for the trimer and tetramer in Figure 6. The binding energies of the neutral and ionic clusters, as deduced from the measured ionization and appearance potentials, are summarized in Table 1 and Figure 7. In the threshold determination for IPs and APs of naphthalene clusters, it is somewhat difficult to find the exact onset of ionization or metastable fragmentation

TABLE 1: Experimental Binding Energies (D_0) and Evaporation Energies (E_{evp}) of the Neutral and Ionic Clusters of Naphthalene, Obtained from the Measured Ionization Potentials (IP) and Appearance Potentials (AP)

$(C_{10}H_8)_n$	IP(n) (eV)	AP(n) (eV)	$E_{evp}(n)$ (meV)	$E_{evp}^+(n)$ (meV)	$D_0(n)$ (meV)	$D_0^+(n)$ (meV)
1	8.135(1)[a]					
2	7.58(4)	8.26(3)	125(40)	680(40)	125	680
3	7.56(3)	7.83(2)	250(30)	270(30)	375	950
4	7.49(3)	7.73(3)	150(30)	220(30)	525	1150

[a] The values in parentheses indicate a standard deviation (1σ).

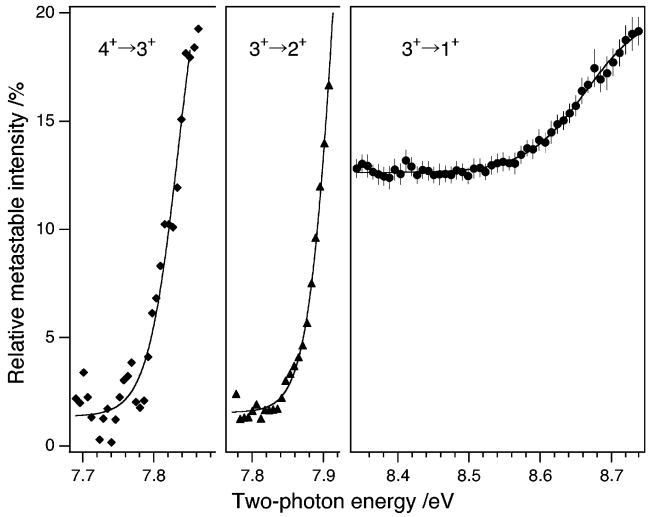

Figure 6. Appearance potentials of the naphthalene cluster ions corresponding to the evaporation of neutral molecule(s) as a function of two-photon energy. The experimental data points are normalized to the respective intensities of the parent ions which are partially collected in the ARTOF spectrometer.

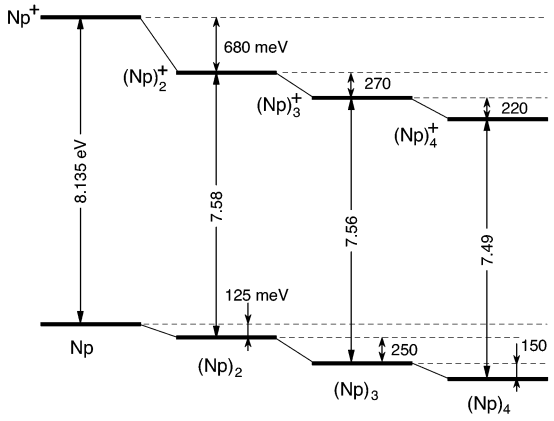

Figure 7. Schematic energy diagram of the neutral and ionic clusters of naphthalene pertaining to the respective evaporation energies deduced from the measured ionization and appearance potentials.

thresholds due to slow increase in ion current with increasing photon energy in the vicinity of threshold. Assuming a model function (sigmoid) for the rise of ion current from a flat background, it is however possible to estimate the onset of ionization and fragmentation with meaningful uncertainties. The standard deviations (σ) in Table 1 are based on such fitting procedure.

Several interesting observations are evident from the results in Table 1. First, the binding energy of the naphthalene trimer (375 meV) is about three times the dimer binding energy (125 meV). Experiment (rotational coherence spectroscopy[13]) as well as computation (MP2/6-31G[14]) have shown that the naphthalene

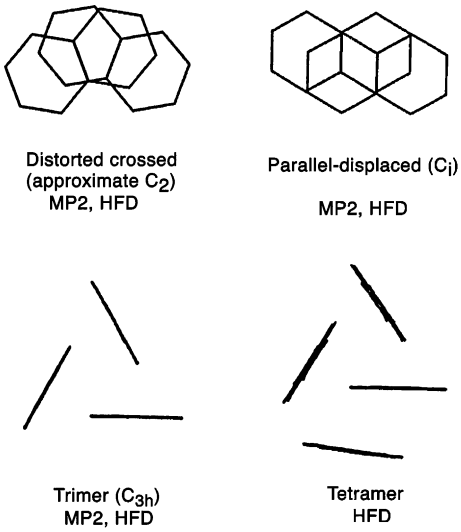

Figure 8. Minimum-energy MP2/6-31G and HFD/6-31G structures of the neutral dimer and trimer of naphthalene and the HFD/6−31 G structure of naphthalene tetramer.

trimer has C_{3h} cyclic structure in which the three long axes of the monomers lie parallel to the C_3 symmetry axis, Figure 8. Assuming that only the pairwise interactions contribute to the interaction energy, the binding energy of the trimer is expected to be three times that of the dimer, as observed in experiment. Thus, many-body interactions do not appear to be an important contributor to the binding energy of the cyclic naphthalene trimer. Second, while the binding energy of the neutral naphthalene dimer (125 meV) is much larger than that of the neutral benzene dimer (70 meV), the binding energies of the respective dimer cation are very similar. Third, the evaporation energy of the naphthalene tetramer (150 meV) is significantly smaller than that for the naphthalene trimer (250 meV). For the ionic clusters, the evaporation energies of the trimer (270 meV) and tetramer ions (220 meV) are small as compared to the evaporation energy of the dimer ion (680 meV). Fourth, the binding energy of the naphthalene dimer ion (680 meV) is close to half the energy of the near-infrared absorption band (530 meV),[15] which represents the electronic transition from the bound charge resonance state to the repulsive charge resonance state at higher energy (vide infra).

Discussion

Franck—Condon Factor for the Photoionization of the Electronically Excited Neutral Clusters. The slow increase in the dimer photoionization yield with increasing photon energy, near the threshold (Figure 4), has an important implication on the geometry of the dimer cation relative to the electronically excited neutral dimer. It is known that the two-photon ionization of the naphthalene dimer proceeds via the two-step process involving excimer formation from the photo-excited dimer, followed by one-photon ionization of the excimer.[12,16] As the time scale of the excimer formation (picoseconds) is much shorter than the nanosecond time scale of the competing electronic relaxation processes,[17] the efficiency of the excimer formation is essentially unity over the range of the $S_1 \leftarrow S_0$ excitation energies. Thus, the photoionization yield of the dimer depends only on the Franck−Condon factor for the photoionization of the excimer. Since this Franck−Condon factor in turn depends on the equilibrium geometry of the dimer cation relative to that of the excimer, the slow increase in the photoionization yield with increasing photon energy implies that

the geometrical structure of the dimer cation is significantly different from the fully overlapping sandwich-pair (D_{2h}) geometry of the excimer.[18] This conclusion is consistent with the partially overlapping, V-shaped, dimer ion of naphthalene proposed by Nishi and co-workers[15] on experimental grounds. The valence-band- (VB-) based model potential of Bouvier et al.[5] predicts two low-energy structures for the naphthalene dimer ion: sandwich-staggered (crossed) and sandwich-eclipsed (sandwich pair). Photoionization of the excimer to the ionic state of the sandwich-staggered conformer would have unfavorable Franck−Condon factor, whereas that to the ionic state of the sandwich-eclipsed would have favorable Franck−Condon factor. The supposition that the conformational difference between the excimer and the ground-state dimer cation is responsible for the small Franck−Condon factor for the excimer-mediated photoionization is supported by the increasing efficiency of the photoionization with increasing photon energy.[19]

The slow increase in the photoionization yield with increasing photon energy, which is also evident for the higher clusters of naphthalene (Figure 4), can be rationalized in a similar way. Previous work from this laboratory[12,20,21] has shown that the excimer clusters, $(C_{10}H_8)_n^*$, as well as the ground-state cation clusters, $(C_{10}H_8)_n^+$, with $n = 2-7$, are composed a strongly bound dimer core, where the electronic excitation or the positive charge is localized, to which the remaining naphthalene molecules are weakly bound, viz., $(C_{10}H_8)_2^*\cdot(C_{10}H_8)_{n-2}$ and $(C_{10}H_8)_2^+\cdot(C_{10}H_8)_{n-2}$. The preference for the dimer core structure of the electronically excited clusters (excimer clusters) and the ionic clusters has been attributed to the excitation resonance ($A^*A \leftrightarrow A\ A^*$) stabilization of the excimer[12,20] and the charge resonance ($A^+A \leftrightarrow AA^+$) stabilization of the dimer cation.[7,10,15,21] If the excimer core in the electronically excited neutral clusters and the dimer ion core in the ionic cluster have significantly different geometries, the Franck−Condon factor for the excimer-mediated photoionization of the neutral clusters would be small as in the case of the naphthalene dimer. Interestingly, the increase in the ion current with increasing photon energy, near threshold, is significantly smaller for excitation of the $\bar{8}^1$ level ($0^0 + 399\ cm^{-1}$) that lies below the energy threshold for excimer formation, than for excitation of the $\bar{7}^1$ level ($0^0 + 871\ cm^{-1}$) that lies above it, Figure 5. This is reasonable since the ionization transition from the cyclic structure of the S_1 trimer to the (partially) overlapping structure of the ionic state would be less efficient as compared to the photoionization of the overlapping dimer core structure (of the excimer cluster) to the ionic state.[11]

Charge Resonance Interactions and Binding Energy of the Dimer Cations. Comparison of the measured binding energy of the dimer cation with the transition energy of its charge resonance (CR) absorption provides valuable insights into the site symmetry of the dimer ion and the nature of the dominant attractive force leading to bonding.[15,21] The bonding in dimer cations arises largely form ion-neutral electrostatic interaction and intermoiety CR interaction, $A^+A \leftrightarrow AA^+$. The energies of the dimer ion states are therefore lowered by the electrostatic interaction E_{es}, then, split by CR interaction (E_{CR}), as illustrated in the scheme below:

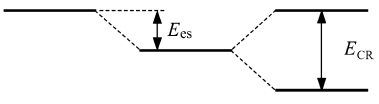

The magnitude of the CR interaction can be spectroscopically probed by measuring the energy of the near-infrared absorption band that represents the electronic transition from the bound CR state (ψ_+) to the repulsive CR state (ψ_-) of higher energy[15,21]

$$\psi_\pm = \frac{1}{\sqrt{2}}(|A^+A\rangle \pm |A\ A^+\rangle).$$

If the contribution of the electrostatic interaction to the total binding energy is small relative to the contribution from the CR interaction, and if the two moieties in the dimer ion are symmetry equivalent, the binding energy of the dimer cation is simply half the transition energy of the CR absorption. Interestingly, half the CR transition energy is indeed equal to the measured binding energy for benzene dimer ion, and close to four-fifths of the measured binding energy for naphthalene dimer ion,[22] Table 2. It may therefore be concluded that the dominant attractive force leading to bonding in naphthalene and benzene dimer ions is charge resonance interaction. The results in Table 2 also imply that the two-monomer moieties in the dimer ions are likely to occupy equivalent sites. The computed low-energy structures of the naphthalene dimer ion[5] as well as those of the benzene dimer ion[5,23] possess two monomers that are site equivalent. It may be significant that the measured binding energy of the naphthalene dimer ion (680 meV) is similar to that (856 meV) computed using the VB-based model potential.[5]

TABLE 2: Comparison of the Measured Binding Energy (D_0^+) of the Dimer Cation with Half of the Transition Energy (ΔE) of the Charge Resonance Band

	λ_{CR} (nm)[a]	$^1/_2\Delta E_{CR}$ (meV)	D_0^+ (meV)
$(benzene)_2^+$	920[b]	670	660,[c] 665[d]
$(naphthalene)_2^+$	1180[e]	530	680[f]

[a] Wavelength maximum of the CR absorption band. [b] Reference 22. [c] Reference 6. [d] Reference 8. [e] Reference 15. [f] This work.

The conclusion that the CR interaction is the dominant source of the binding energy is at odds with the high-pressure mass spectrometry of Meot-Ner,[24] which indicates that the CR contribution to the total binding energy is about 35% for the benzene dimer ion and 21% for the naphthalene dimer ion. Moreover, the binding energies obtained from the high-pressure mass spectrometry[24,25] are substantially larger than those based on the measurements of the ionization and appearance potentials in a supersonic jet. The reasons for these discrepancies are not known. However, because of the high sensitivity and good *S*/*N* ratio, the binding energies determined from the jet experiment are believed to be reasonably accurate.

Comparison of the Measured and Computed Binding Energies of Neutral Clusters. Several ab initio calculations of the low-energy structures of the neutral dimer of naphthalene are available in the literature.[2−4,26] All of them utilize the second-order Møller−Plesset (MP2) theory with bases sets that vary in size, polarization, and diffuseness. The two lowest-energy structures predicted by these calculations are a distorted crossed geometry of approximate C_2 symmetry, which is the global minimum, and C_i parallel-displaced dimer of slightly higher energy,[26] Figure 8. Interestingly, the MP2 calculation with a small basis set (6-31G), and without the counterpoise (CP) correction,[2,26] yields binding energies ($D_e = 225$ meV) that are closest to the experimental value ($D_0 = 125$ meV). The MP2/6-31G* (0.25) and MP2/aug-cc-pVDZ calculations yield binding energies that are too large by a factor of 5 without the CP correction and by a factor of 3 with the CP correction.

Agreement with the experimental binding energy is significantly better for the binding energies (114 meV) of the neutral dimer computed by the VB-based model potential.[5] However,

since the global minimum (T-shaped) predicted by the method differs from that based on all other methods (MPs, HFD, and exp-6-1), significance of the energy agreement is not at all clear at present.

Core Structures of the Neutral and Ionic Clusters. The fact that the evaporation energy of the neutral tetramer is similar to that of the dimer (Table 1) has relevance to the likely geometry of the naphthalene tetramer. Mass-selective and ionization-loss stimulated Raman spectra, measured by Felker and co-workers, have shown that the naphthalene tetramer has four inequivalent sites.[27] Furthermore, the analyses of the spectral splitting and red shift of the $\bar{8}_0^1$ band by Saigusa and Lim[28] indicate that the tetramer has a nearly overlapping dimeric sites that are surrounded by two monomers. The intermoiety excitonic interaction has been proposed to be strong only between the pair of molecules occupying the dimeric site.[28] These conclusions are consistent with the minimum-energy HFD/6-31G structure of the tetramer, Figure 8, in which the fourth naphthalene moiety is attached to one of the monomers in the C_{3h} cyclic trimer motif in a slip-parallel dimerlike arrangement.[29] The energy required for the evaporation of the fourth molecule from such a structure (150 meV) would be similar to the evaporation energy of the dimer (125 meV), as observed in experiment (Table 1). The preference for the trimer core structure of the neutral tetramer can be traced to the exception stability of the C_{3h} cyclic conformer of the neutral trimer. The similar evaporation energy of the trimer ion (270 meV) and tetramer ion (220 meV) is consistent with the conclusion[21] that the ionic clusters of naphthalene, $(C_{10}H_8)_n^+$, $n = 2-7$, are composed of a strongly bound dimer ion core to which the remaining neutral naphthalene molecules are weakly bound, viz., $(C_{10}H_8)_2^+ \cdot (C_{10}H_8)_{n-2}$. For the trimer and tetramer ions of such a structure, the evaporation energy (the energy required for the removal of the one neutral monomer) would be essentially independent of the cluster size.

Conclusion

In summary, the results presented in this paper lead to several interesting conclusions pertaining to the neutral and ionic clusters of aromatic hydrocarbons. First, the slow increase in the photoionization of the neutral dimer with increasing photon energy, near threshold, indicates that there is a substantial geometry charge in going from the excited state of the dimer (excimer) to the ground state of the dimer ion. This leads to the relatively small Franck−Condon factors for the ionization of the excimer. Second, the observation that the measured binding energy of the dimer ion is very close to half the transition energy of the charge resonance absorption, in the near-infrared, suggests that the dimer cations of benzene and naphthalene are stabilized mostly by charge resonance interactions. Third, the measured evaporation energy of the neutral tetramer, which is very similar to that of the neutral dimer, is consistent with the HFD/6-31G geometry of the tetramer in which the fourth naphthalene molecule attaches to one of the monomers in the C_{3h} cyclic trimer motif in a slip-parallel dimerlike arrangement. Finally, the very similar evaporation energies of the trimer and tetramer ions of naphthalene support the dimer core structures of the ionic clusters in which the positive charge is localized in the strongly bound dimer core.

Acknowledgment. We are grateful to the Office of the Basic Energy Sciences of the U.S. Department of Energy for support of this work.

References and Notes

(1) See, for a recent summary: Lee, N. K.; Park, S.; Kim, S. K. *J. Chem. Phys.* **2002**, *116*, 7902.
(2) Gonzalez, C.; Lim, E. C. *J. Phys. Chem. A* **2000**, *104*, 2953.
(3) Lee, N. K.; Park, S.; Kim, S. K. *J. Chem. Phys.* **2002**, *116*, 7910.
(4) Walsh, T. R. *Chem. Phys. Lett.* **2002**, *363*, *45*.
(5) Bouvier, B.; Brenner, V.; Millié, P.; Soudan, J.-M. *J. Phys. Chem. A* **2002**, *106*, 10326.
(6) Krause, B.; Ernstberger, B.; Neusser, H. J. *Chem. Phys. Lett.* **1991**, *184*, 411.
(7) Ernstberger, B.; Krause, H.; Kiermeier, A.; Neusser, H. J. *J. Chem. Phys.* **1990**, *92*, 5285.
(8) Grover, J. R.; Waiters, E. A.; Huit, E. T. *J. Phys. Chem.* **1987**, *91*, 3233.
(9) Stockburger, M.; Gattermann, H.; Klusmann, W. *J. Chem. Phys.* **1975**, *63*, 4519.
(10) Kühlewind, H.; Neusser, H. J.; Schlag, E. W. *Int. J. Mass Spectrom. Ion Phys.* **1983**, *51*, 255.
(11) Saigusa, H.; Sun, S.; Lim, E. C. *J. Chem. Phys.* **1992**, *97*, 9072.
(12) Saigusa, H.; Lim, E. C. *Acc. Chem. Res.* **1996**, *29*, 171 and references therein.
(13) Benharash, P.; Gleason, M. J.; Felker, P. M. *J. Phys. Chem. A* **1999**, *103*, 1442.
(14) Gonzalez, C.; Lim, E. C. *J. Phys. Chem. A* **1999**, *103*, 1437.
(15) Inokuchi, Y.; Ohashi, K.; Matsumoto, M.; Nishi, N. *J. Phys. Chem.* **1995**, *99*, 3416.
(16) Saigusa, H.; Lim, E. C. *Chem. Phys. Lett.* **1993**, *211*, 410.
(17) Saigusa, H.; Lim, E. C. *Chem. Phys. Lett.* **2001**, *336*, 65.
(18) Sadygov, R. G.; Lim, E. C. *Chem. Phys. Lett.* **1994**, *225*, 441.
(19) Fujiwara, T.; Lim, E. C. Unpublished work.
(20) Saigusa, H.; Sun, S.; Lim, E. C. *J. Phys. Chem.* **1992**, *96*, 10099.
(21) Saigusa, H.; Sun, S.; Lim, E. C. *J. Phys. Chem.* **1994**, *98*, 13470.
(22) Ohashi, K.; Nishi, N. *J. Phys. Chem.* **1992**, *96*, 2931.
(23) Miyoshi, E.; Ichikawa, T.; Sumi, T.; Sakai, Y.; Shida, N. *Chem. Phys. Lett.* **1997**, *275*, 404.
(24) Meot-Ner, M. *J. Phys. Chem.* **1980**, *84*, 2724.
(25) Hiraoka, K.; Fujimaki, S.; Aruga, K.; Yamabe, S. *J. Chem. Phys.* **1991**, *95*, 8413.
(26) Gonzalez, C.; Lim, E. C. *J. Phys. Chem. A*, submitted.
(27) Schaeffer, M. W.; Kim, W.; Maxton, P. M.; Romascan, J.; Felker, P. M. *Chem. Phys. Lett.* **1995**, *242*, 632.
(28) Saigusa, H.; Lim, E. C. *J. Chem. Phys.* **1995**, *103*, 8793.
(29) Gonzalez, C.; Lim, E. C. *Chem. Phys. Lett.* **2002**, *357*, 161.